Chemical Physics Letters 586 (2013) 97–99

Contents lists available at ScienceDirect

Chemical Physics Letters

journal homepage: www.elsevier.com/locate/cplett

Quinoid conjugated dye designed for efficient sensitizer in dye sensitized solar cells

Yang Jiao, Wei Ma, Sheng Meng *

Beijing National Laboratory for Condensed Matter Physics and Institute of Physics, Chinese Academy of Sciences, Beijing 100190, China

ARTICLE INFO

Article history:
Received 20 June 2013
In final form 2 September 2013
Available online 18 September 2013

ABSTRACT

Paraquinoid rings are introduced in the π-conjugation of all-organic donor-π-acceptor dyes as sensitizer in dye sensitized solar cells, to drastically shift optical response from violet-blue to near-infrared and to significantly enhance photoabsorption. Taking Y1 as a model, real time electron dynamics simulations based on time-dependent density functional theory confirm that paraquinoid conjugation maintains high thermal stability and ultrafast electron-hole separation at ambient temperature.

Introduction

Dye sensitized solar cells (DSCs), as one of most promising low-cost alternatives to crystalline solar cells, have received intensified attention since the work by O'Regan and Grätzel in 1991 [1]. Thousands of dye molecules have been tested and much progress have been made [2]. High efficiencies are usually achieved with expensive metal complexes as dye sensitizers notable for their ability to harvest solar irradiation extending to near infrared (IR) region [3,4]. Only recently efficiencies over 13% have been reported using modified Zn-porphyrin dye coadsorbed with metal-free dye Y123 [5]. All organic metal-free dyes have advantages of non-toxicity, ease to synthesis, low cost and high extinction coefficients, producing energy conversion efficiency >10% [6]. Since metal-free dyes usually have light absorption in shorter wavelength range than metal-complex competitors, tremendous efforts have been devoted to modify dye's absorption in near-IR solar irradiance. For example, by replacing dye's donor with stronger electron attributors such as ullazine group [7], or by employing electron rich π-linkers [8–10].

Here we report theoretical design and characterization of paraquinoid units as the π linker of organic dye to drastically improve optical absorption at near-IR region. The resulted dyes show stability when adsorbed on TiO_2 surface in our theoretical simulations. Real-time time dependent density functional theory (RT-TDDFT) simulations indicate the efficient electron-hole separation at the interface. Dyes with paraquinoid conjugation achieving high light-to-electricity efficiency limit ~20% are predicted with large photocurrents and ultrafast electron injection.

Our study is based on first-principles calculations within density functional theory (DFT) and time-dependent DFT (TDDFT). Quantum mechanical simulations are proven useful to facilitate design and screening of new dyes [11]. Geometry optimization and ab initio molecular dynamics (AIMD) calculations were carried out using PBE exchange-correlation functional with generalized gradient approximation and double-ξ basis with polarization orbitals (DZP) implemented in SIESTA package [12]. The TiO_2 electrode is modeled by a six atomic layer slab with anatase (101) surface, where the bottom three layers are fixed at bulk geometry. A periodicity of 10.24 × 15.13 $Å^2$ and a vacuum layer at least of 10 Å is used. Only Γ-point in reciprocal space is considered. For free standing TiO_2 surface and dye molecules, structure optimization is achieved when forces on atoms are smaller than 0.01 eV/Å. For dye/TiO_2 adsorption systems, a looser criterion of 0.04 eV/Å is used, which does not introduce any noticeable structural changes. AIMD trajectories are produced with a time step of 1 fs at 350 K. Production runs last for 10 ps following equilibration in the first 1 ps. Optical absorption spectra were obtained using TDDFT in GAUSSIAN 09 [13]. Hybrid functional B3LYP and its long-range corrected version CAM-B3LYP are used with 6-31G(d) basis set, which has been tested to give reliable excitation energies for organic molecules [11]. An electron density convergence criterion of 1.0×10^{-4} a.u. is used in all the above mentioned calculations. The coupled electron-ion dynamics of the dye/TiO_2 interface is performed using RT-TDDFT based on Ehrenfest theorem [14]. An electron density convergence criterion of 2.0×10^{-3} a.u. is used in the electronic state evolutions, which guarantees the good stability of the simulations as discussed in reference [14]. This method enables us to directly simulate electron injection, electron-hole separation, and recombination processes in dye solar cells, and provide detailed information about the influence of atomic structure on electron dynamic behaviors.

Dye Y1, with a dimethylaminophenyl donor and cyanoacrylic acceptor, is a small prototype dye representing a typical donor-π-acceptor structure (Figure 1a). It shows maximum absorption at wavelength (λ_{max}) of 378 nm in ethanol and achieves light-to-

* Corresponding author.
E-mail address: smeng@iphy.ac.cn (S. Meng).

0009-2614/$ - see front matter © 2013 Elsevier B.V. All rights reserved.
http://dx.doi.org/10.1016/j.cplett.2013.09.008

electricity energy conversion efficiency of 2.4% [15,16]. We introduce one and two paraquinoid rings in the C=C double bond linker of Y1 to achieve modified Y1b and Y1b2 dyes (Figure 1a). To compare the effects of quinoid and aromatic rings [17] we also utilize one and two paraphenylene rings in the C–C single bond linker of Y1, producing Y1a and Y1a2 dyes (Figure 1a).

Figure 1(b) shows calculated absorption spectra of these dyes. The maximum absorption is mainly attributed to the π–π^* transition from the highest occupied molecular orbital (HOMO) to the lowest unoccupied molecular orbital (LUMO). Both molecular orbitals are distributed all over the dye molecule (see Supplementary Figure S1). The spatial overlap [17] (Λ) between HOMO and LUMO is 0.67 for Y1. The Λ increases to 0.82 and 0.87 for Y1b and Y1b2, but decreases to 0.55 and 0.42 for Y1a and Y1a2. For long dyes with phenyl π-linkers Y1a and Y1a2, long-range corrected functional (CAM-B3LYP) are necessary to describe charge transfer excitation [18] (Supplementary Table S1). The absorption spectra are broadened by GAUSSIAN distribution [19] with full width at half maximum of 4760 cm^{-1}. Calculated spectrum of Y1 matches well with experiment (grey dashed line in Figure 1b) [15]. The paraphenylene linkers tune the spectra for less than 40 nm per increased unit. This value is consistent with previous work [20] where the number (n) of π-units increases from 1 to 10. For paraphenylene insertion, almost no red-shift is observed [15] after $n \geqslant 2$. Other aromatic linkers including thiophene, selenophene and thienothiophene were also analyzed, where a slightly larger red-shift, but still less than 80 nm per unit, was shown [20]. For paraquinoid linkers we found that the red shift is larger than 120 nm (125.5 and 153.4 nm for the first and second unit in the linker). As shown in Figure 1(b) the absorption of Y1b2 extends to 700–900 nm which could compete with absorption of Ru-based black dyes in this region. Moreover, the extinction coefficient is more than 10 times larger than the black dye [21]. With paraquinoid π-linkers, oscillator strengths of dye absorption are enhanced by 30–40% in comparison to that with corresponding aromatic linkers.

Next we examine the adsorption of the dyes on TiO_2 surface. A six atomic layer anatase (1 0 1) slab is used to model TiO_2 surface. The lower three layers are fixed at bulk geometry. Tridentate adsorption configuration is identified to be most stable, similar to the previous finding (Figure 2) [22]. We confirm that surface adsorption results in only a tiny shift (a few nanometers) in λ_{max} (Supplementary Table S2). The interface bonds are shown to be stable at ambient temperature in the 10 ps AIMD simulations. For Y1 on anatase the average interface Ti–N, Ti–O bond lengths are 2.39 ± 0.14 Å and 2.24 ± 0.11 Å, respectively (Supplementary Figure S2).

Figure 2 shows energy level alignment at the dye/TiO_2 interface. The density of states of TiO_2 (blue shadows) and the ground state oxidation potential (E_{ox}) of dyes (green lines) are extracted from the projected density of states of the composite system. The excited state oxidation potential (E^*_{ox}) of dyes (red lines) is estimated by E_{ox} plus the lowest transition energy (E_{0-0}) in TDDFT [23]. The edge of TiO_2 conduction band up-shifts due to increasing interface dipole moments [24], which are 2.838, 4.454, 5.310 e·Å for Y1, Y1b and Y1b2, respectively. The up-shift will benefit DSC device for a larger open circuit voltage (V_{oc}). For all the three dyes the energy alignments satisfy the requirement of DSCs that the E^*_{ox} lies above the E_{CBM}, and the E_{ox} below the redox potential of I^-/I_3^-(−4.8 eV), which will allow efficient electron injection and dye regeneration.

Electron injection dynamics was simulated using real time evolution of dye/TiO_2 upon photoexcitation. An electron in the HOMO of dye is promoted to the LUMO to mimic the first excitation state [14,25]. The distribution of the excited electron and hole on TiO_2 (χ(t)) is tracked, where $\chi = \int dr|\tilde{\psi}(r)|^2$, $\tilde{\psi}(r) = \sum_{j\in TiO_2} c_j|\tilde{\psi}(r)|\ \psi_j(r)$ are the localized numerical atomic orbitals centered at atoms belonging to TiO_2. Configurations sampled from the AIMD trajectory show similar electron injection dynamics (Supplementary Figure S3). Therefore we present one of typical electron injection trajectories for each dye (Figure 3). Electron injection time less than 100 fs for Y1 was observed in ultrafast transient absorption experiment [15]. The calculated value of ~160 fs is on the same scale. The D-quinoid-A dyes also show fast electron injection in 200 fs, faster than the typical thermal relaxation of excited states (a few picoseconds) and other competing processes such as back transfer and dye deexcitation (nanoseconds) [26]. The hole transfer time scale is much larger than the simulation time. The resulting efficiency for photoelectron injection is >90%, indicating photoexcited electrons can inject into TiO_2 without problems for quinoid dyes [27]. The efficient electron injection to TiO_2 will also guarantee the photostability of quinoid dyes against photo-induced damages.

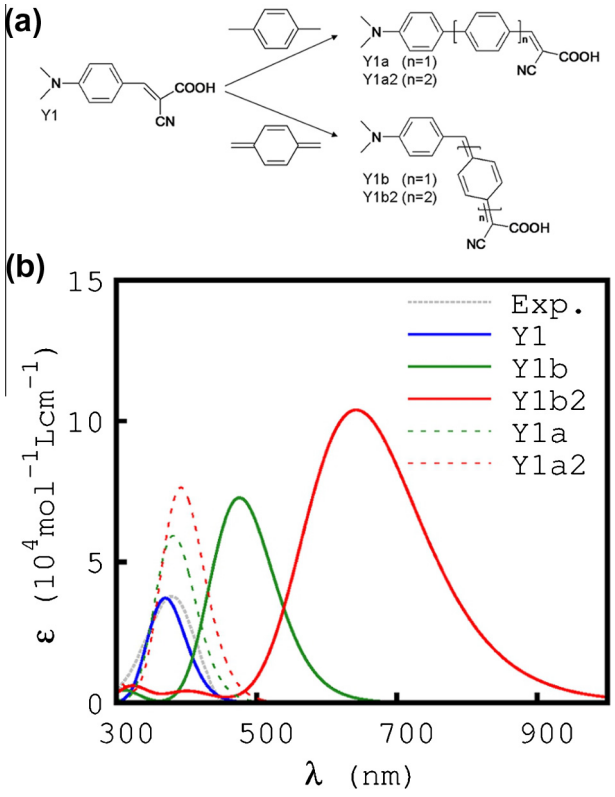

Figure 1. The structures (a) and absorption spectra (b) of dye Y1 and derivatives. The grey dashed line is experimental curve for Y1 [15].

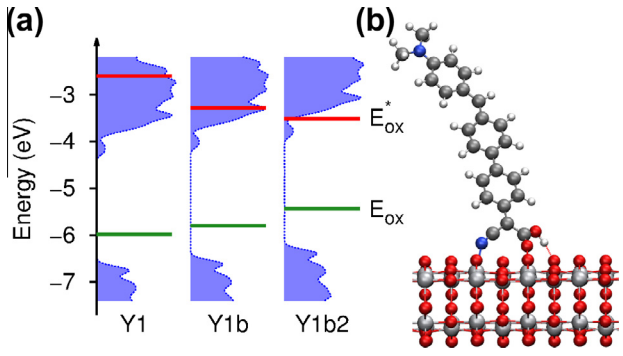

Figure 2. (a) Energy level alignment for the dyes adsorbed on TiO_2 surface. (b) Adsorption structure of Y1b2 on TiO_2 obtained from geometry optimization.

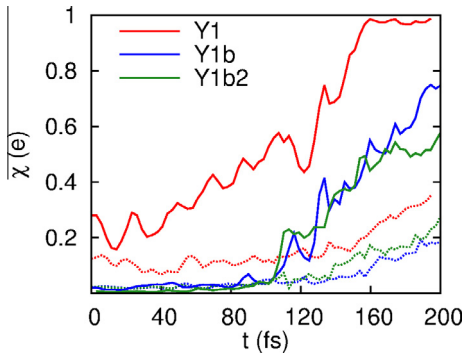

Figure 3. The simulated excited state electron–hole dynamics. The solid lines present the excited electron distribution on the TiO_2 electrode. The dashed lines indicates the distribution of hole.

The small size of the quinoid dyes will benefit photovoltaic performance of DSCs. For triphenylamine-based L-dyes the λ_{max} reaching a value close to Y1b (463 nm) [28] is achieved by conjugation with two polyene and two thiophene units in the π-linker, hence the length of the dye is about 10 Å longer than Y1b. Device practice shows that longer dyes largely deteriorate dye diffusion and adsorption in nanoporous materials, and result in faster recombination with electrolyte due to the lack of compact protective dye layers onto TiO_2 surface. We expect Y1b and Y1b2 dyes have a low recombination rate (close to that for a dye of similar size, L1 or JD21) [7,28] while present significantly improved sunlight harvest efficiency. Moreover, as the red-shift quickly saturates with increasing aromatic π linker [20], intense absorption at a large λ_{max} similar to that of Y1b2 cannot be achieved with conventional wisdom.

To show the promise of quinoid conjugation, we estimate energy conversion efficiency of DSCs employing these dyes. The short circuit current (I_{sc}) can be evaluated by integrating the overlap between dye optical absorption and solar spectral irradiance (SI):

$$I_{SC} = q \iint \frac{SI}{hc/\lambda} \epsilon \rho e^{-\epsilon \rho x} d\lambda dx \qquad (1)$$

where q is the electron charge, ρ the concentration of adsorbed dyes, x the depth of the mesoporous layer. We assume TiO_2 thickness to be 10 μm, and $\rho = 300$ mmol L^{-1} [28]. The I_{sc} are predicted to be 3.7, 15.2 and 36.0 mA cm^{-2} for Y1, Y1b, and Y1b2 dyes, respectively, assuming unity efficiency for electron injection and collection. The theoretical maximum limit of V_{OC} could be calculated by the difference between the CBM and redox potential of I^-/I_3^-(−4.8 eV). Using typical values of fill factors (0.7), this leads to an overall efficiency limit of 1.0%, 5.6%, 19.2% for Y1, Y1b, and Y1b2 dyes, respectively. The experimental solar cell performance of Y1 shows I_{SC} = 4.3–5.6 mA cm^{-2} and total efficiency of 2.2–2.4% [15]. We notice that the onset of experimental IPCE extends to 560 nm, inducing a larger I_{SC}. The redshift of IPCE onset could be a result of solvent effect, which will be addressed in our future work. According to the theoretical prediction, advantages of using quinoid dyes are obvious. We expect the experimental synthesis of these dyes be straightforward. Indeed, D-quinoid-A dyes have been widely synthesized and studied in nonlinear optics [29]. Near infrared absorption with maximum absorption peak in the range of 700–900 nm was also realized [30]. Quinoid dyes similar to Y1b and Y1b2 with two dimethylaminophenyl as donor and two cyano group as acceptor have been synthesized and are proved to be stable at ambient condition and in polar solvent [30].

In summary we propose modifying D-π-A organic dyes with paraquinoid rings as π-conjugation. This extension of π-conjugation will generate remarkable bathochromic shift (from violet to near IR) and strong oscillation strengths. Theoretical simulations on the dye/TiO_2 interface demonstrate the adsorption stability and efficient electronic couplings. Characterizing the electronic and dynamic properties indicates they act as highly effective light sensitizers with predicted high energy conversion efficiency limit close to 20%.

Acknowledgments

We acknowledge financial supports from NSFC (grants 11222431 and 11074287), MOST (2012CB921403), and hundred-talent program of CAS.

Appendix A. Supplementary data

Supplementary data associated with this article can be found, in the online version, at http://dx.doi.org/10.1016/j.cplett.2013.09.008.

References

[1] B. O'Regan, M. Grätzel, Nature 353 (1991) 737.
[2] A. Mishra, M.K.R. Fischer, P. Bäuerle, Angew. Chem. Int. Ed. 48 (2009) 2474.
[3] F. Gao et al., J. Am. Chem. Soc. 130 (2008) 10720.
[4] Y. Cao et al., J. Phys. Chem. C 113 (2009) 6290.
[5] A. Yella et al., Science 334 (2011) 629.
[6] W. Zeng et al., Chem. Mater. 22 (2010) 1915.
[7] J.H. Delcamp, A. Yella, T.W. Holcombe, M.K. Nazeeruddin, M. Grätzel, Angew. Chem. Int. Ed. 52 (2013) 376.
[8] R. Chen, X. Yang, H. Tian, X. Wang, A. Hagfeldt, L. Sun, Chem. Mater. 19 (2007) 4007.
[9] H. Tian, X. Yang, R. Chen, R. Zhang, A. Hagfeldt, L. Sun, J. Phys. Chem. C 112 (2008) 11023.
[10] J. Zhang, H.-B. Li, S.-L. Sun, Y. Geng, Y. Wu, Z.-M. Su, J. Mater. Chem. 22 (2012) 568.
[11] M. Pastore, E. Mosconi, F. De Angelis, M. Grätzel, J. Phys. Chem. C 114 (2010) 7205.
[12] J.M. Soler, E. Artacho, J.D. Gale, A. García, J. Junquera, P. Ordejón, D. Sánchez-Portal, J. Phys.: Condens. Matter 14 (2002) 2745.
[13] See Supplementary material for reference details.
[14] S. Meng, E. Kaxiras, J. Chem. Phys. 129 (2008) 054110.
[15] T. Kitamura et al., Chem. Mater. 16 (2004) 1806.
[16] N.A. Anderson, T. Lian, Annu. Rev. Phys. Chem. 56 (2005) 491.
[17] S. Manzhos, H. Segaw, K. Yamashita, Chem. Phys. Lett. 527 (2012) 51.
[18] M. Pastore, E. Mosconi, F. De Angelis, M. Gratzel, J. Phys. Chem. C 114 (2010) 7205.
[19] (a) S. I. Gorelsky, SWizard program, http://www.sg-chem.net/, University of Ottawa, Ottawa, Canada, 2012.;
(b) S.I. Gorelsky, A.B.P. Lever, J. Organomet. Chem. 635 (2001) 187.
[20] I. Ciofini, T. Le Bahers, C. Adamo, F. Odobel, D. Jacquemin, J. Phys. Chem. C 116 (2012) 11946.
[21] Md. K. Nazeeruddin, P. Pèchy, M. Grätzel, Chem. Commun. (1997) 1705.
[22] Y. Jiao, F. Zhang, M. Grätzel, S. Meng, Adv. Funct. Mater. 23 (2013) 424.
[23] M. Pastore, S. Fantacci, F. De Angelis, J. Phys. Chem. C 114 (2010) 22742.
[24] J. Krüger, U. Bach, M. Grätzel, Adv. Mater. 12 (2000) 447.
[25] S. Meng, E. Kaxiras, Nano Lett. 10 (2010) 1238.
[26] A. Hagfeldt, G. Boschloo, L. Sun, L. Kloo, H. Pettersson, Chem. Rev. 110 (2010) 6595.
[27] M. Komatsu, K. Tamaki, J. Nakazaki, S. Uchida, T. Kubo, H. Segawa, ECS Trans. 16 (2009) 65.
[28] D.P. Hagberg et al., J. Org. Chem. 72 (2007) 9550.
[29] Y.-L. Wu, F. Bureš, P.D. Jarowski, W.B. Schweizer, C. Boudon, J.-P. Gisselbrecht, F. Diederich, Chem. Eur. J. 16 (2010) 9592.
[30] N.A. Zaidi, M.R. Bryce, G.H. Cross, Tetrahedron Lett. 41 (2000) 4645.